Supplementary material for Bussell, Dangerfield, Gilligan & Cunniffe, 2019, Applying optimal control theory to complex epidemiological models to inform real-world disease management, *Phil. Trans. R. Soc. B.*

# Electronic Supplementary Material — Model Details

E.H. Bussell, C.E. Dangerfield, C.A. Gilligan & N.J. Cunniffe

---

## 1 Full details of the models

We here describe the full details of the simulation model, and of both approximate models. The simulation model and its parameters are arbitrary, but intended to represent a scenario in which an accurate simulation model can be built and fitted to the real disease system in question. The model itself includes features abstracted from metapopulation or network epidemic models as routinely used for plant, animal and human diseases [1–5].

### 1.1 Simulation model

The simulation models transmission of infection between individuals across a network of nodes. Nodes are positioned randomly in three separate regions, with 20 nodes in regions A and C, and 15 nodes in region B. The nodes are positioned such that no two nodes are closer than a predetermined threshold, here 0.2 spatial units. The connectivity between nodes within a region is calculated using an exponential kernel with a scale parameter $\alpha$ of 0.2 units ($\sigma_{ij} = \beta e^{-d_{ij}/\alpha}$) where $d_{ij}$ is the distance between nodes $i$ and $j$. Between regions, three connections are made between the closest pairs of nodes in regions A and B, and B and C, with a coupling value of $0.1\beta$ for each. There are no connections between regions A and C.

Each node contains a total of 30 hosts, with on average 10% of these being in the high risk group of individuals. The exact number in each risk class for each node is chosen using a binomial trial, giving heterogeneity in the risk structure across the network. Each individual host can be in one of three active states (figure S1): susceptible ($S$), infected ($I$) or vaccinated ($V$), or removed ($R$) by the disease. Throughout superscripts refer to the risk group (high: H, low: L), and subscripts identify the node. For example, $S_3^{\mathrm{H}}$ represents the total number of high risk susceptibles in node 3. In addition, we use $N$ to refer to the total number of active hosts, such that $N_3^{\mathrm{H}}$ is the number of susceptible, infected and vaccinated high risk hosts in node 3.

Trajectories are simulated using the Gillespie direct method [6]. The possible events are host birth and death, infection, vaccination, and removal and recovery of infected hosts. These events and the associated rates are given in Table S1. Parameters, as specified in Table S2, were chosen to give a large epidemic under no control intervention, spreading across all three regions. Typical simulation trajectories with no control are shown in Figure S2.

| Event | State Change | Rate |
|---|---|---|
| Birth | $\emptyset \to S_i^r$ | $bN_i^r$ |
| Death | $\{S_i^r, I_i^r, V_i^r\} \to \emptyset$ | $dN_i^r$ |
| Infection | $S_i^r \to I_i^r$ | $S_i^r \sum_{j,r'} \sigma_{ij} \rho^{rr'} I_j^{r'}$ |
| Vaccination | $S_i^r \to V_i^r$ | $f_i^r \eta_{\max} S_i^r / N_i^r$ |
| Removal | $I_i^r \to \emptyset$ | $\mu I_i^r$ |
| Recovery | $I_i^r \to S_i^r$ | $\nu I_i^r$ |

Table S1: Possible events in the simulation model with associated rates.

| Meaning | Parameter | Default Value |
|---|---|---|
| Birth Rate | $b$ | $0.01\,\mathrm{t}^{-1}$ |
| Death Rate | $d$ | $0.01\,\mathrm{t}^{-1}$ |
| Maximum Vaccination Rate | $\eta_{\max}$ | $200\,\mathrm{hosts\,t}^{-1}$ |
| Removal Rate | $\mu$ | $0.5\,\mathrm{t}^{-1}$ |
| Recovery Rate | $\nu$ | $0.25\,\mathrm{t}^{-1}$ |
| Risk Coupling | $\begin{pmatrix} \rho^{\mathrm{HH}} & \rho^{\mathrm{HL}} \\ \rho^{\mathrm{LH}} & \rho^{\mathrm{LL}} \end{pmatrix}$ | $\begin{pmatrix} 1.0 & 0.008 \\ 0.008 & 0.016 \end{pmatrix}$ |
| Spatial Coupling | $\sigma$ | *see text* |
| Transmission Rate | $\beta$ | $2.5\,\mathrm{host}^{-1}\,\mathrm{t}^{-1}$ |

Table S2: Parameter values used for simulation model trajectories.

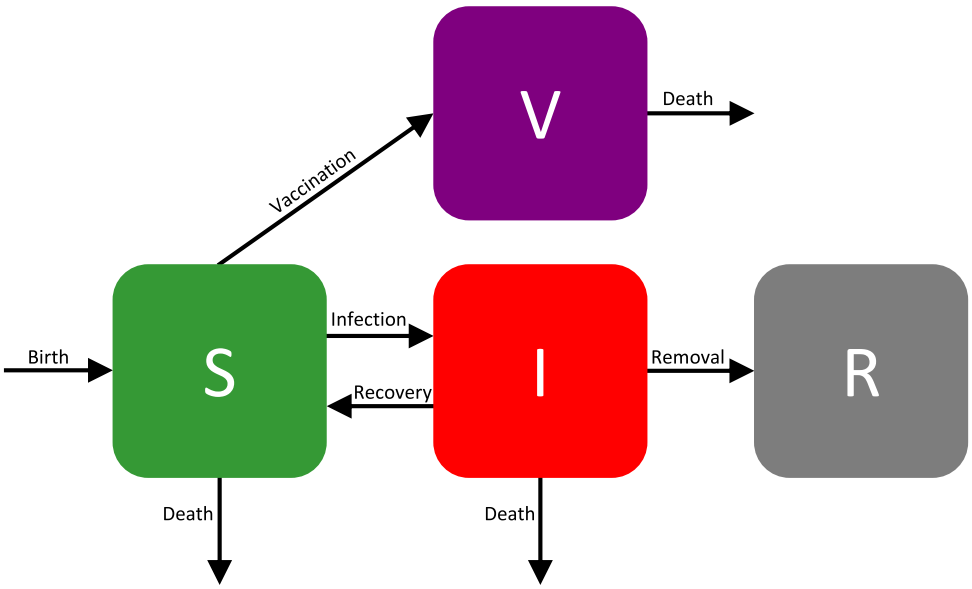


Figure S1: Diagram of host states and transitions. For transition rates see Table S1

## 1.2 Risk based approximate model

This model factors out all spatial information from the simulations, and approximates the resulting risk structure using a set of ordinary differential equations. The ODE system has one equation for each of the six host states: susceptible, infected and vaccinated in the high risk ($S^{\mathrm{H}}, I^{\mathrm{H}}, V^{\mathrm{H}}$), and low risk groups ($S^{\mathrm{L}}, I^{\mathrm{L}}, V^{\mathrm{L}}$). For risk group $r$, the full system of equations is given by:

$$\begin{aligned}
\dot{S}^r &= bN^r - dS^r - S^r\left(\hat{\rho}^{r\mathrm{H}}I^{\mathrm{H}} + \hat{\rho}^{r\mathrm{L}}I^{\mathrm{L}}\right) - \frac{f^r\eta_{\max}S^r}{N^r} + \nu I^r \\
\dot{I}^r &= -dI^r + S^r\left(\hat{\rho}^{r\mathrm{H}}I^{\mathrm{H}} + \hat{\rho}^{r\mathrm{L}}I^{\mathrm{L}}\right) - \mu I^r - \nu I^r \\
\dot{V}^r &= -dV^r + \frac{f^r\eta_{\max}S^r}{N^r}
\end{aligned} \tag{1}$$

where $\hat{\rho}$ is a $2\times 2$ matrix giving the approximated risk structure, i.e. the rate at which each risk group infects each other risk group. All other parameters are the same as in the simulation model. The risk structure must be approximated since the exact spatial structure is not modelled, whereas all other parameters are specific to individual hosts and so can be lifted from the simulation model. The state values are mapped from the simulations simply by summing all hosts in that state across the whole network (e.g. $S^r = \sum_i S_i^r$).

## 1.3 Spatial approximate model

This model includes regional spatial information as well as risk structure. This gives 18 possible states: susceptible, infected and vaccinated across risk groups (high and low), and regions ($A$, $B$ and $C$). The states here are summed across nodes within a region (e.g. $S_A^r = \sum_{i\in A} S_i^r$). For risk group $r \in \{\mathrm{H}, \mathrm{L}\}$, and region

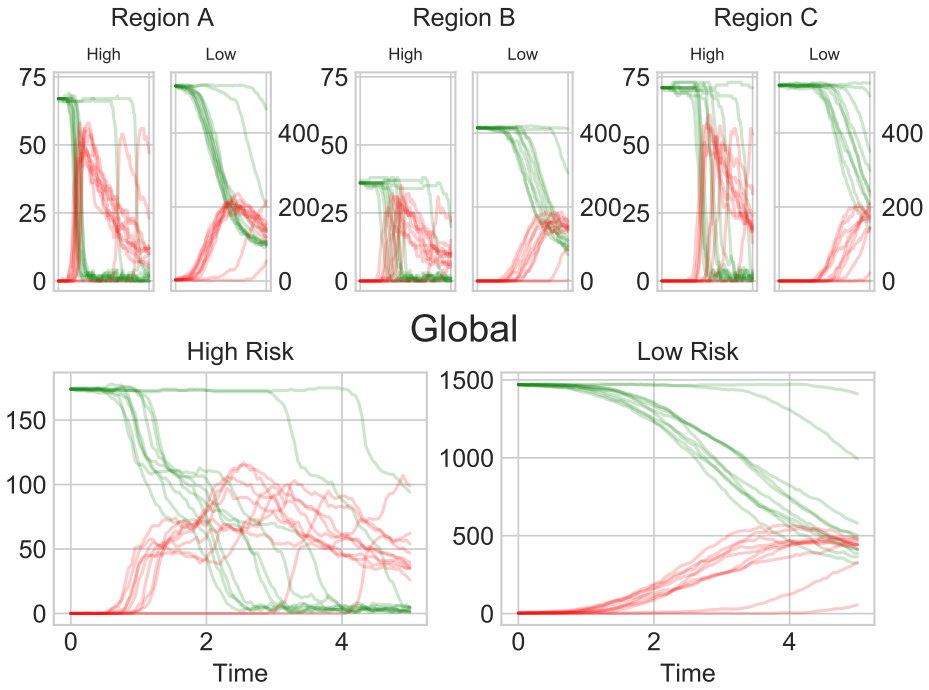


Figure S2: Ten typical simulation model trajectories with no control. Green and red lines represent susceptible and infected hosts respectively.

$X \in \{A, B, C\}$, the system of differential equations is given by:

$$\begin{aligned}
\dot{S}^r_X &= bN^r_X - dS^r_X - S^r_X \sum_{X' \in \{A,B,C\}} \tilde{\sigma}_{XX'} \left( \tilde{\rho}^{r\mathrm{H}} I^{\mathrm{H}}_{X'} + \tilde{\rho}^{r\mathrm{L}} I^{\mathrm{L}}_{X'} \right) - \frac{f^r_X \eta_{\max} S^r_X}{N^r_X} + \nu I^r_X \\
\dot{I}^r_X &= - dI^r_X + S^r_X \sum_{X' \in \{A,B,C\}} \tilde{\sigma}_{XX'} \left( \tilde{\rho}^{r\mathrm{H}} I^{\mathrm{H}}_{X'} + \tilde{\rho}^{r\mathrm{L}} I^{\mathrm{L}}_{X'} \right) - \mu I^r_X - \nu I^r_X \qquad (2) \\
\dot{V}^r_X &= - dV^r_X + \frac{f^r_X \eta_{\max} S^r_X}{N^r_X} .
\end{aligned}$$

The $3 \times 3$ matrix $\tilde{\sigma}$ approximates spatial coupling between regions, and $\tilde{\rho}$ is a $2 \times 2$ matrix giving the approximated risk structure.

## 1.4 Model fitting

To fit the risk based model to the simulation model the 4 parameters in $\hat{\rho}$ must be chosen. We fit these using maximum likelihood estimation, computing the likelihood as the product of contributions from 200 realisations of the simulation model with no interventions. Each individual event within a realisation occurring after a time $\delta t$ contributes a factor $\delta L_i$ to the likelihood:

$$\delta L_i = r_k \mathrm{e}^{-\sum r_i \delta t}$$

where the $r_i$ are the rates of all possible events, and $r_k$ is the rate of the event that actually occurs. The full likelihood is the product of all $\delta L_i$ across all realisations.

The same fitting procedure is used to fit $\tilde{\rho}$ and $\tilde{\sigma}$ in the space based model. Here there are a total of 13

parameters, but we set $\tilde{\rho}^{\mathrm{HH}}$ to one to ensure a unique solution (since the infection rate is proportional to the product of $\tilde{\rho}$ and $\tilde{\sigma}$). We also set the coupling between regions $A$ and $C$ ($\tilde{\sigma}_{AC}$ and $\tilde{\sigma}_{CA}$) to zero, as well as from $B$ into $A$ and from $C$ into $B$. This is because the epidemic spreads from $A$ to $B$ to $C$, and backward spread is negligible. This leaves a total of 8 parameters to fit.

Fits to simulation data are shown for the risk based model in figure S3, and in figure S4 for the space based model. To verify the optimisation we generated profile likelihoods plots [7], shown in figures S5 and S6. The risk model captures the median risk dynamics well. The highly stochastic nature of spread between regions however, means the spatial model does not capture the timings of introductions accurately.

The best-fitting spatial deterministic model leads to disease progress curves in regions B and C that rise more quickly than the mean of the stochastic simulations, although the epidemic size within each region closely matches the simulations. This is because it is impossible for a deterministic model where the rates are fitted via maximum likelihood to adequately capture the dynamics of an epidemic in which the following three conditions are satisfied:

(i) there is initially no infection;

(ii) there is a very small force of infection into the region;

(iii) there are relatively fast within-region dynamics once disease has entered.

These conditions are true inside regions B and C and so we see reduced rate of spread in the stochastic case. This effect is due to stochastic fade outs after introduction events, as well as negative covariance between susceptible and infected hosts, leading to reduced infection rates in the simulations [8, pp. 227–229 and pp. 238–240]. Figure S7 demonstrates that this effect is seen in the simplest case of a metapopulation model with no risk structure. The rates are directly lifted from simulation to approximation to show the effect is purely due to the difference between deterministic and stochastic analogues. We also tested that our fitting procedures give these same values (data not shown).

The spatial approximate model could be extended and improved to account for these effects, for example by making use of moment closure techniques [9] or nonlinear force of infection terms [10] as used by Clarke *et al*. [11] and Stroud *et al*. [12], but we here focus on simplicity. Despite the limitations of the deterministic models, our proposed control frameworks allow the resulting controls to be used practically and successfully, particularly when approximating models are repeatedly reset. Since the benefits of the control frameworks should not depend on the exact fitting process used, we also fitted both approximate models by minimising the sum of squared errors from the simulation disease progress curves. For the risk based model the following sum of squared errors was minimised:

$$\mathrm{SSE} = \sum_{i,j} \left(\Delta I_i^{\mathrm{H}}(t_j)\right)^2 + \left(\Delta I_i^{\mathrm{L}}(t_j)\right)^2 \tag{3}$$

where $\Delta I_i^{\mathrm{r}}(t_j)$ is the difference in the number of infected host in risk group $r$ between the approximate model and simulation realisation $i$ at time $t_j$. The sum is over all simulation realisations and across 51 times over the simulation time. The equivalent SSE function was used for the spatial approximate model, but summing differences for each region as well. Using this alternative fitting process did not change the ordering of control strategies as seen in Figure 3 in the main text (data not shown).

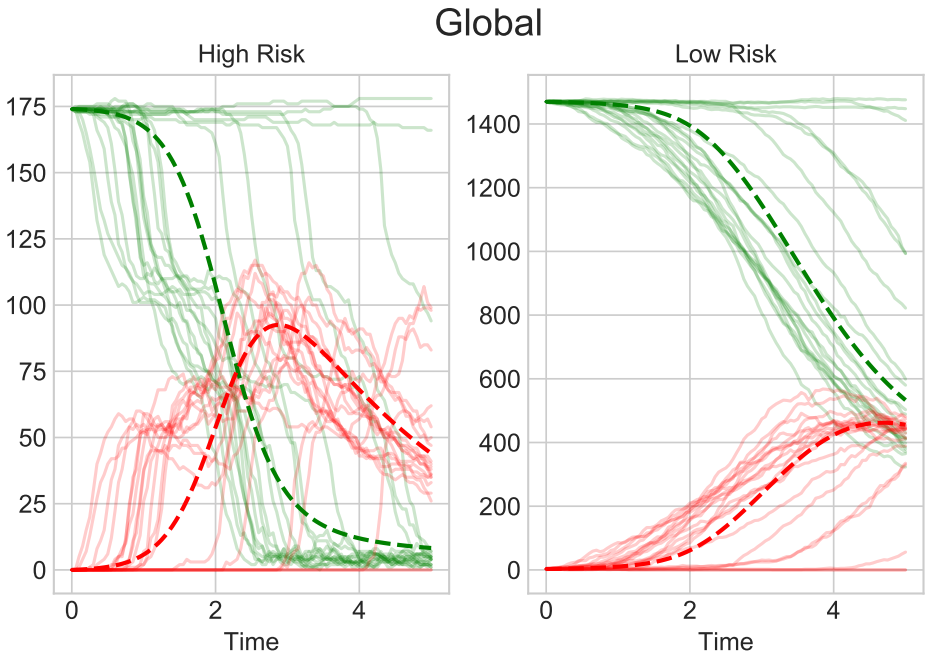


Figure S3: Fits to simulation data for the risk based model. Dashed lines show the risk model, and faded lines show 20 of the simulation runs. Green and red lines represent susceptible and infected hosts respectively.

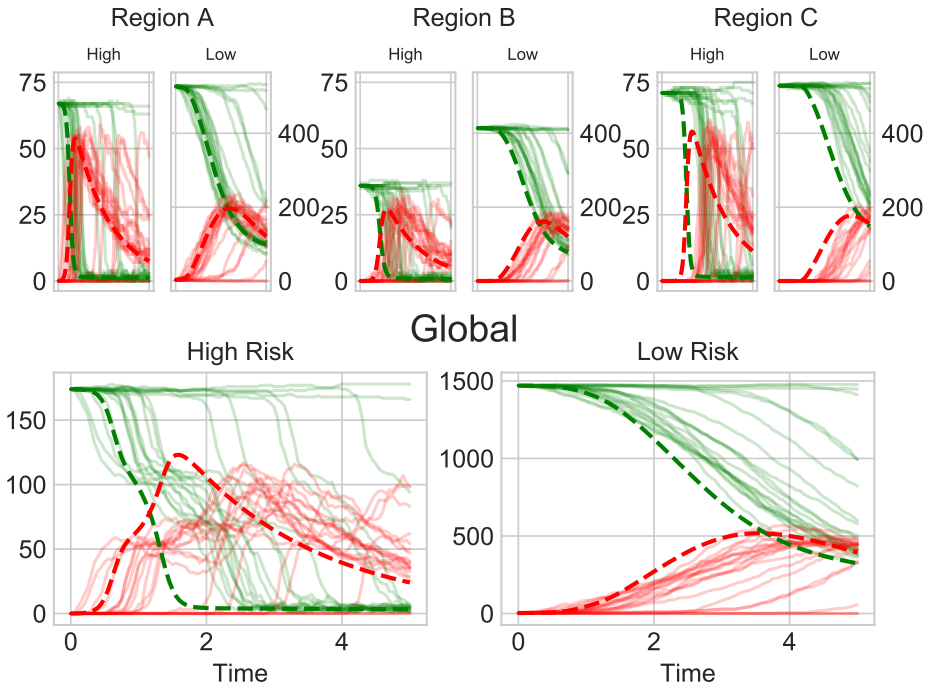


Figure S4: Fits to simulation data for the space based model. Dashed lines show the space model, and faded lines show 20 of the simulation runs. Green and red lines represent susceptible and infected hosts respectively. We note that the approximate dynamics are faster than those in the simulations. This effect is explained in the text.

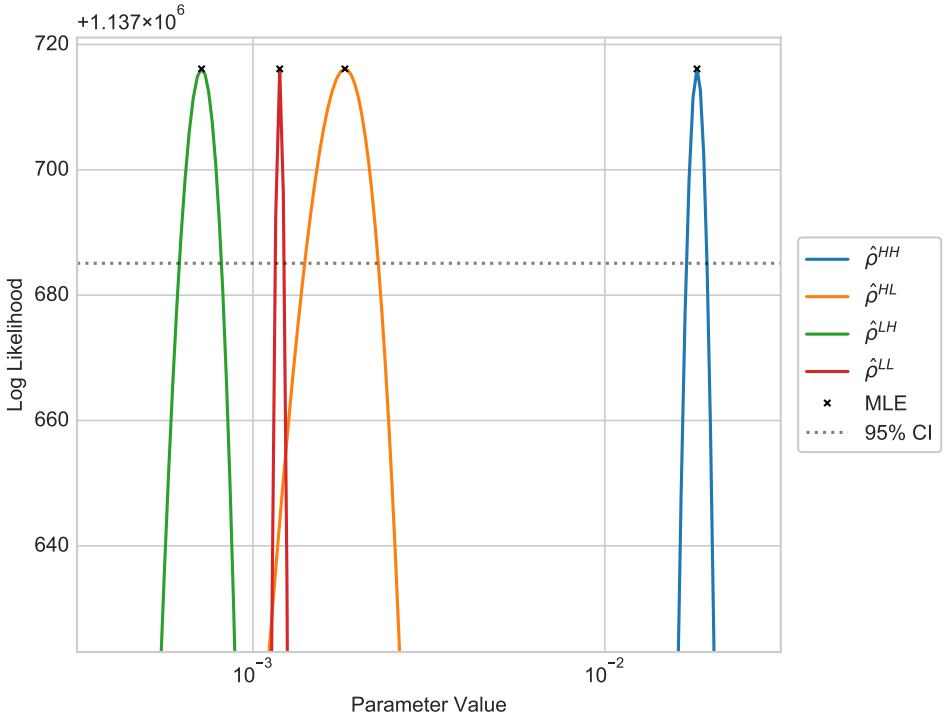


Figure S5: Profile likelihood analysis for the risk based approximate model. The offset ($1.137 \times 10^6$) must be added to all values on the y axis. The profile for every parameter crosses the 95% confidence interval threshold, ensuring identifiability of each parameter. In all cases maximum likelihood estimates coincide with the maximum along the profile.

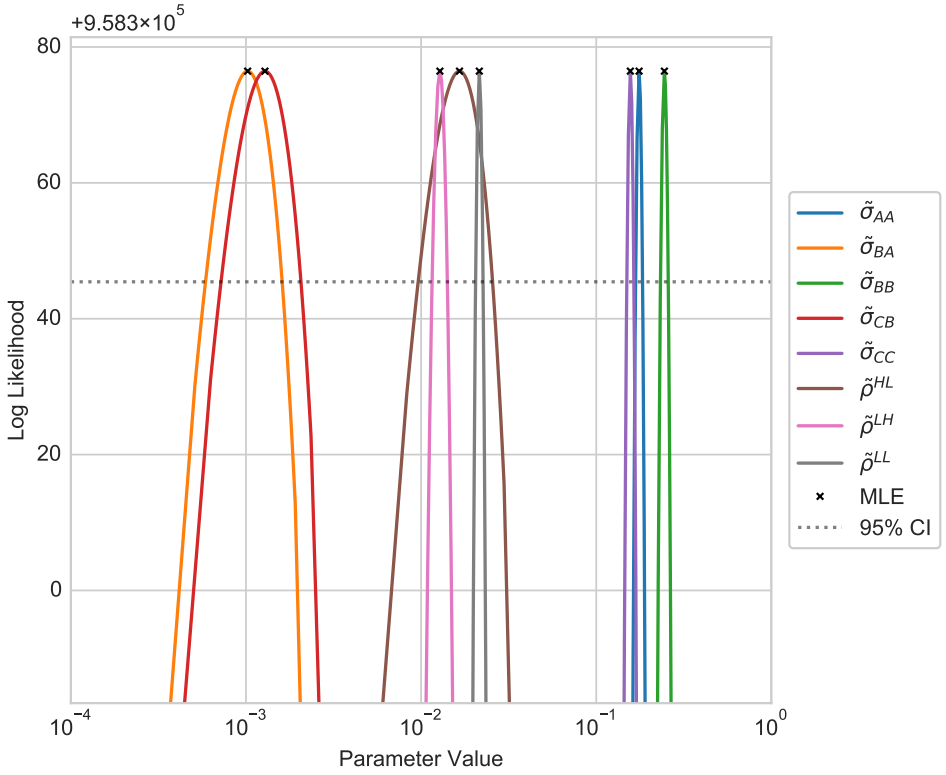


Figure S6: Profile likelihood analysis for the space based approximate model. The offset ($9.583 \times 10^5$) must be added to all values on the y axis. The profile for every parameter crosses the 95% confidence interval threshold, ensuring identifiability of each parameter. In all cases maximum likelihood estimates coincide with the maximum along the profile.

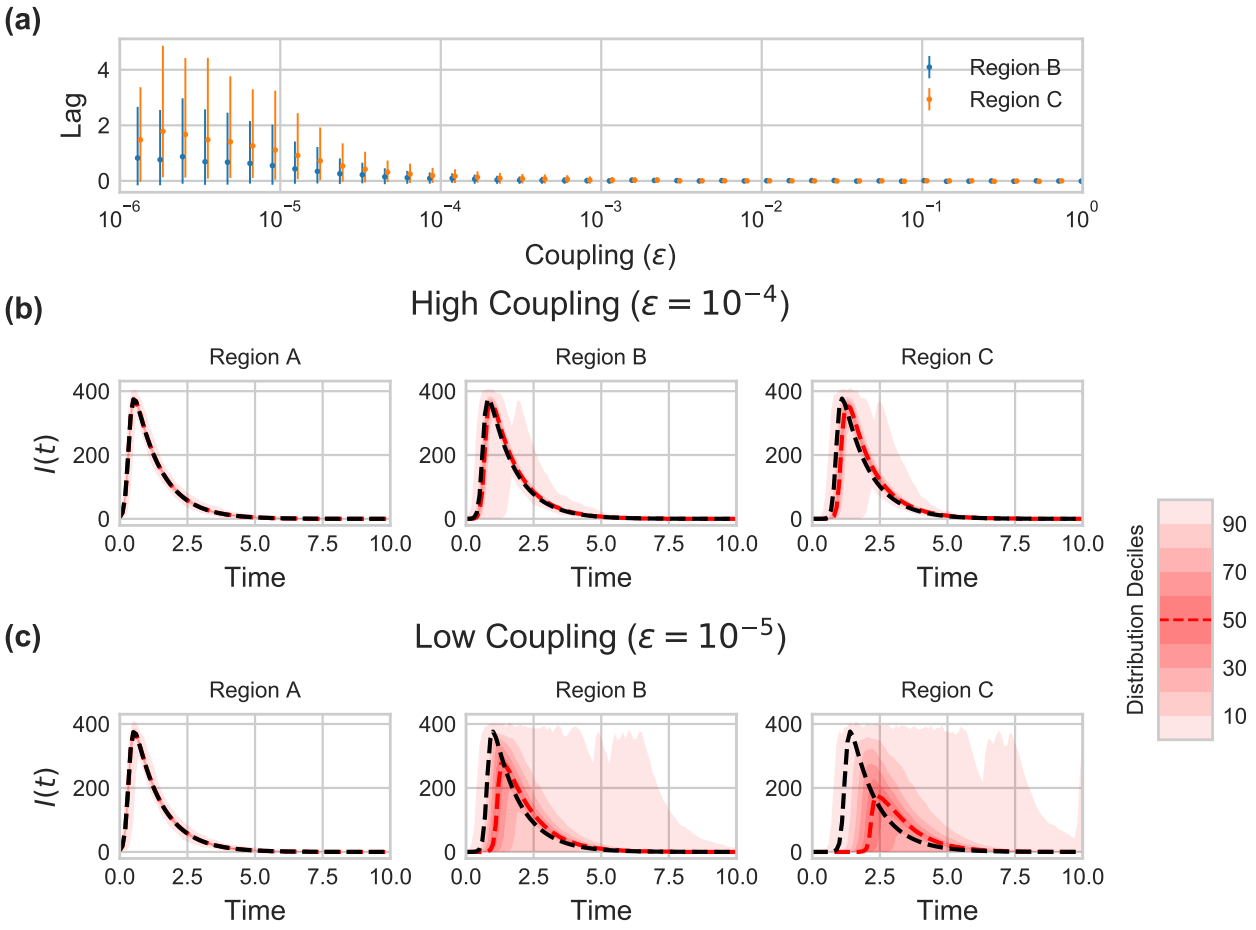


Figure S7: Illustration of increased rate of spread in deterministic models when coupling is small. In this figure we use a 3 patch metapopulation model, with well-mixed dynamics within regions and coupling between regions A and B, and B and C. There is no risk structure. **(a)** shows the difference in peak infection time for deterministic and stochastic versions of the model with identical rates. Positive values indicate the deterministic model peaks earlier. Dots give the mean of 1000 stochastic simulations, with error bars showing the 95th percentile. **(b)** shows median stochastic dynamics and deciles in red, and deterministic disease progress curve in black, for a high coupling value ($10^{-4}$). The same is shown in **(c)** for a low coupling value ($10^{-5}$)

# 2 Control strategy testing

## 2.1 Control optimisation and lifting

Control optimisation is carried out using the numerical optimisation software BOCOP v2.0.5 [13] for both the risk and space based models. BOCOP takes the dynamics and objective function and optimises the control using a direct transcription approach. This approach discretises both state and control and optimises the values of both as a nonlinear programming problem [14]. We chose this optimisation method due to its simplicity and robust convergence properties, but the control frameworks we discuss in the main paper are not limited to this method. Other numerical methods could be used, as well as indirect approaches such as the forward-backward sweep method [15]. For further discussion of numerical approaches to optimal control problems see [14].

When lifting controls to the simulation model resources are allocated such that all individuals within the targeted group have an equal probability of being vaccinated. With the risk based model, resources are allocated across all nodes and susceptible individuals in the targeted risk group are selected randomly. In the space based model resources are spread over nodes in the targeted region. Again, the probability of selecting any single susceptible host is constant. This amounts to weighting the resource allocated to a particular node by its total population.

## 2.2 Strategy Details

The 'user-defined' strategies vaccinate either the high risk group, or both risk groups with a constant proportion of resources allocated to the high risk hosts. This proportion is chosen by scanning over its value, running 1000 realisations of the simulation model in each case to assess its performance (figure S8). The proportion that gives the lowest mean objective value is found to be 63% to the high risk group, and this value is used in the main text. As can be seen in figure S8 the optimum occurs in a very broad minimum, so whilst we can be confident that splitting resources is preferable to the 'High' strategy the precise value of the optimal split is uncertain. Since the precise value has little effect on the epidemic cost (hence the broad minimum), we simply use 63% as a representative value. The 'user-defined' strategies are constant in time and do not target hosts based on location. When lifted to the simulation model resources are spread across nodes such that any individual susceptible host in a risk group has an equal probability of being vaccinated, as with lifting of risk based controls.

As explained in the main text, the open-loop strategies optimise the relevant approximate model giving an estimated optimal control strategy as a function of time. This function is used throughout the simulation run, allocating resources as specified by the OCT results. In the MPC strategies, at the update times the approximate model is reinitialised at the current state of the simulation. For example, at update time $t_1$ the number of susceptibles in region A in the approximate model is set by $S_A^{\mathrm{H}}(t_1) = \sum_{i \in A} S_i^{\mathrm{H}}(t_1)$, and similar for other risk groups and regions, and at each update time. The control is optimised going forward from this initial condition and this control is then lifted back to the simulation until the next update time (Algorithm 1). The control is updated every 0.5 time units.

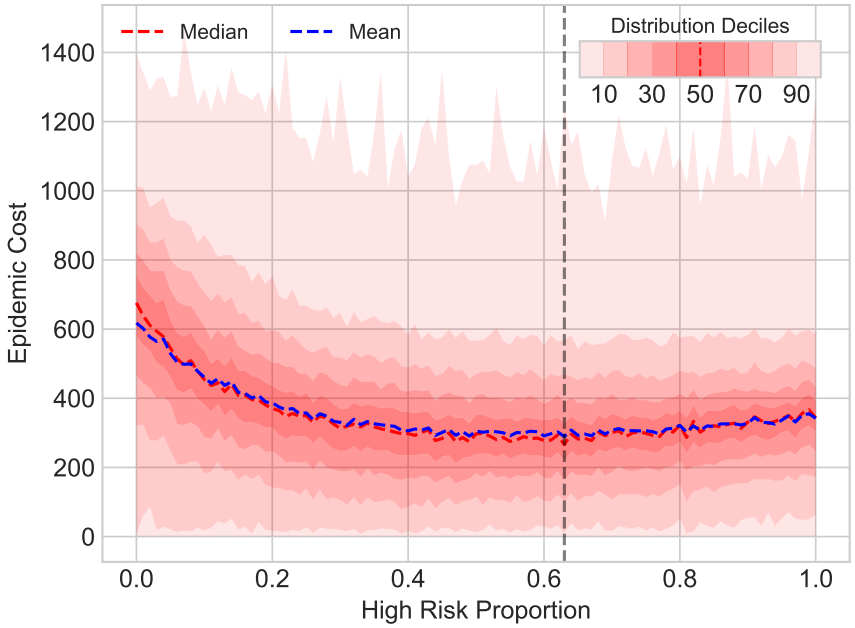


Figure S8: Scan of objective values for 1000 simulations, varying the proportion of control that is allocated to the high risk group. Remaining control is allocated to the low risk group. The optimal allocation to the high risk group is found to be 63%. Deciles in the objectives are shown by the gradient in colour.

**Algorithm 1** MPC and open-loop algorithms. Open-loop simulates for the full time (i.e. step 2–6), whereas MPC re-optimises the control at the update times (step 2–7 with repeated loops back to step 4).

1. Fit simulation model to real data
2. Set initial conditions for simulation model
3. Fit approximate model to simulation data
4. Initialise approximate model at current simulator state
5. Optimise control on approximate model
6. Lift control to simulation model and simulate forward
7. If MPC then at next update time go to step 4

The open-loop risk model optimal control treats high risk individuals early in the epidemic (figure S9a). The strategy then switches to vaccinating both high and low risk hosts, with the majority of control resources allocated to the low risk group. There is then a further switch to vaccinating just the low risk group. The spatial optimal control shows a very similar allocation to risk groups across time (figure S9b), but shifts these allocations across regions as the epidemic spreads through the network (figure S9c).

To generate the objective distributions in Figure 3 of the main text, the simulation model is run 250 times with each control scheme. The cumulative distributions of all simulation runs under each of the strategies are shown in Figure S10 to support the figure in the main text. Figure S11 shows why there is little difference between the risk based open-loop and MPC strategies. The switch time from vaccinating high to low risk individuals that gives the lowest epidemic cost occurs in a broad minimum. This means that the small adjustments made by the

MPC strategy do not have a large effect upon the objective values. In the spatial case however, the introduction times into regions B and C are very variable (figure S2), and so the potential to change which region is being vaccinated can have a large effect on the objective. This means spatial MPC is a significant improvement over open-loop.

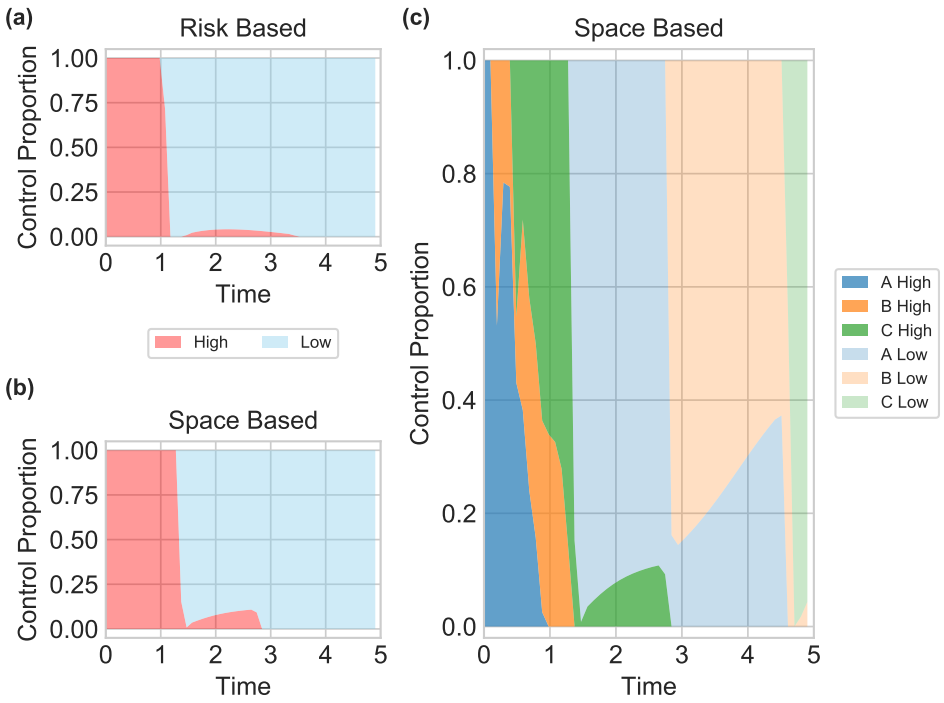


Figure S9: Comparison of open-loop optimal control strategies. **(a)** shows the optimal allocation of control resources to high and low risk groups in the risk based approximate model. **(b)** shows the equivalent for the space based approximate model. This allocation is broken down further in **(c)**, showing the distribution across regions and risk groups for the space based model.

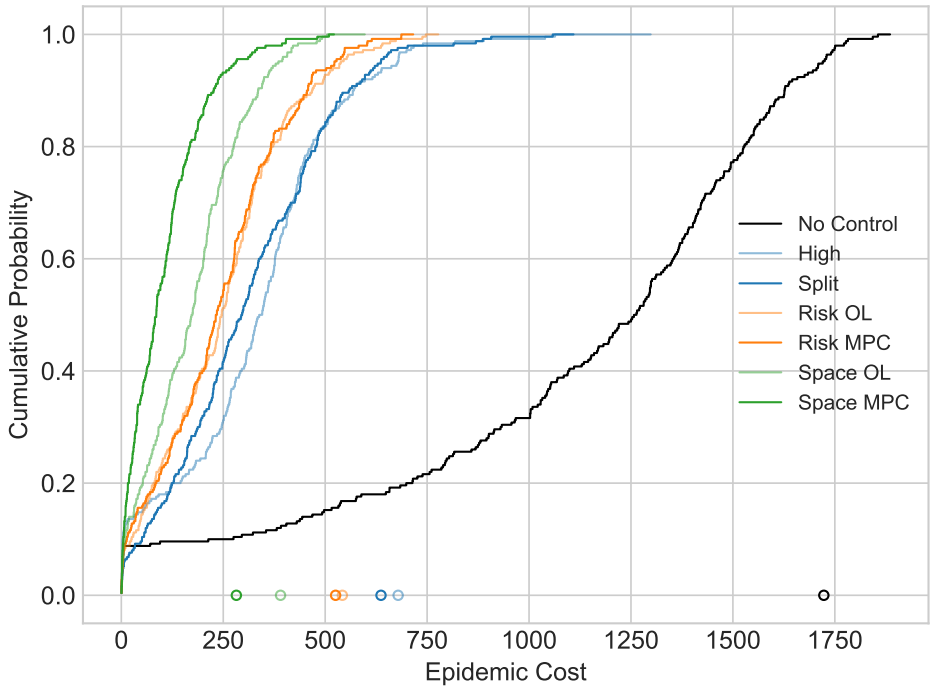


Figure S10: Cumulative distributions of simulation objective values under the tested control strategies. The circles indicate the 95th percentile objective value for each strategy.

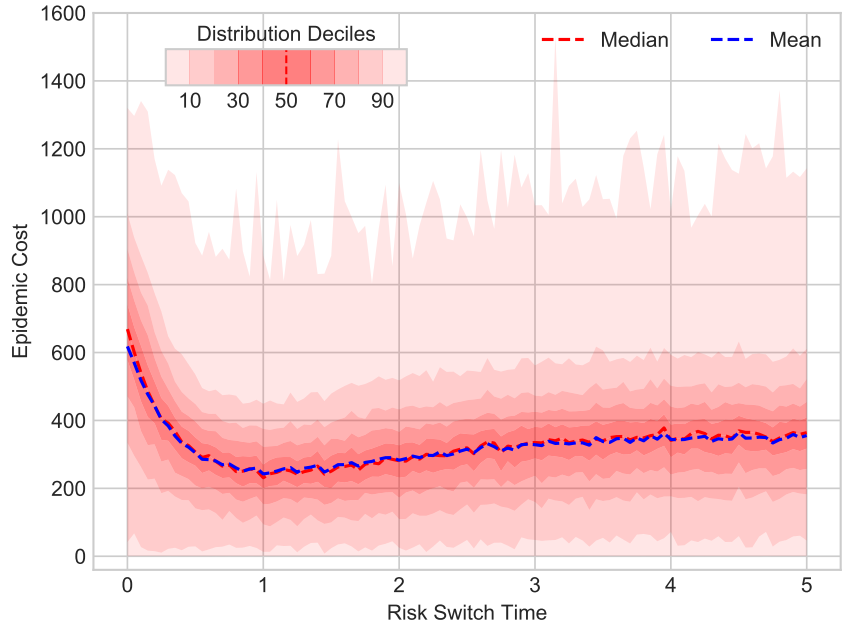


Figure S11: Scan over switch time showing distribution of objective values for 1000 simulations at each time. The switch time specifies when the control stops vaccinating only high risk hosts, and starts vaccinating only low risk hosts. Deciles in the objectives are shown by the gradient in colour.

# 3 Parameter Robustness

As explained in the main text, the MPC framework is expected to provide improved control regardless of the exact form taken by the model or objective function. This does, however, rely on using an appropriately accurate approximate model. We tested a range of arbitrary but reasonable parameter sets, and in all cases the spatial MPC framework performs best in our illustrative model. To illustrate this in a concrete setting we explore systematic adjustments to the risk structure used in the simulation model, but leave more complete exploration of parameter space for future work.

The risk structure is defined by the matrix $\rho$ which in the standard simulation model is given by:

$$\rho = \begin{pmatrix} \rho^{\mathrm{HH}} & \rho^{\mathrm{HL}} \\ \rho^{\mathrm{LH}} & \rho^{\mathrm{LL}} \end{pmatrix} = \begin{pmatrix} 1.0 & 0.008 \\ 0.008 & 0.016 \end{pmatrix} \tag{4}$$

We make the system more homogeneous or more heterogeneous by respectively doubling or halving $\rho^{\mathrm{HL}}$, $\rho^{\mathrm{LH}}$ and $\rho^{\mathrm{LL}}$. That is, the two alternative matrices used are:

$$\begin{aligned} \rho_{\mathrm{hom}} &= \begin{pmatrix} 1.0 & 0.016 \\ 0.016 & 0.032 \end{pmatrix} \\ \rho_{\mathrm{het}} &= \begin{pmatrix} 1.0 & 0.004 \\ 0.004 & 0.008 \end{pmatrix} \end{aligned} \tag{5}$$

Using these values we then scale the transmission rate parameter, $\beta$, such that the mean epidemic cost under no control is within 1% of that using the standard risk structure. The values were found to be 1.49 and 4.30 for the more homogeneous and heterogeneous cases respectively, compared with 2.5 for the default risk structure. The value of $\rho^{\mathrm{HH}}$ is left equal to one without loss of generality since the whole matrix is scaled by $\beta$. The means we only vary the relative transmission rates.

For each new $\rho$ matrix, we rerun the full analysis described above and in the main text, assessing the same six control scenarios with refitted approximate models. Two main effects can be investigated using this analysis. Firstly, the ordering in performance of the six control scenarios can be compared with the ordering using the default risk structure, $\rho$. Secondly the performance of each strategy can be compared with the same strategy using $\rho$. We now look at each of these in turn.

For $\rho_{\mathrm{hom}}$, the more homogeneous case, we find that the order of the control scenarios is unchanged (figure S12). As before we find that spatial MPC leads to the best performance, as found for the default $\rho$. The more heterogeneous case results in a different ordering of control strategy performance (figure S13). The ordering of the 'user-defined' and risk based strategies is as before, but when using $\rho_{\mathrm{het}}$ the spatial open-loop scenario leads to worse performance than the risk based strategies. This is because for this parameter set, and approximate model, the resulting strategies cannot respond to the variability in regional introduction times and control is then targeted at the wrong regions. Importantly though, the spatial MPC strategy reduces average epidemic costs below those of all other strategies. Here the feedback strategy can greatly improve disease management, despite the limitations of the standard open-loop approach. This is similar to the effect seen by Forster and Gilligan [16], where inaccuracies in the switch times lead to ineffective control, but here the feedback loop has mitigated this issue.

We now consider the second effect, namely relative performance of each strategy under the different risk structures (figure S14). For $\rho_{\mathrm{hom}}$, the 'user-defined' and risk based strategies have higher epidemic costs than

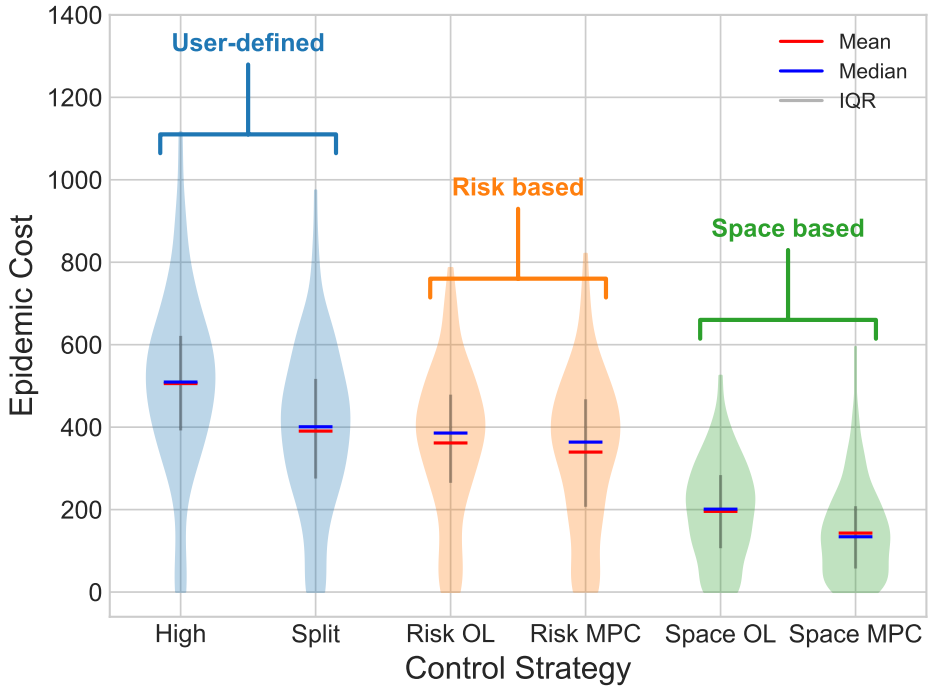


Figure S12: Results of control optimisation scenarios with alternative, more homogeneous risk structure $\rho_{\text{hom}}$.

were found with the default risk structure, $\rho$. This is because with a more homogeneous system, risk is less important and so the risk based strategies are less powerful. Using $\rho_{\text{het}}$ the risk based strategies perform relatively better because of the increased importance of risk structure in the simulations. There is little change in epidemic cost for the spatial open-loop strategy using all three risk structures.

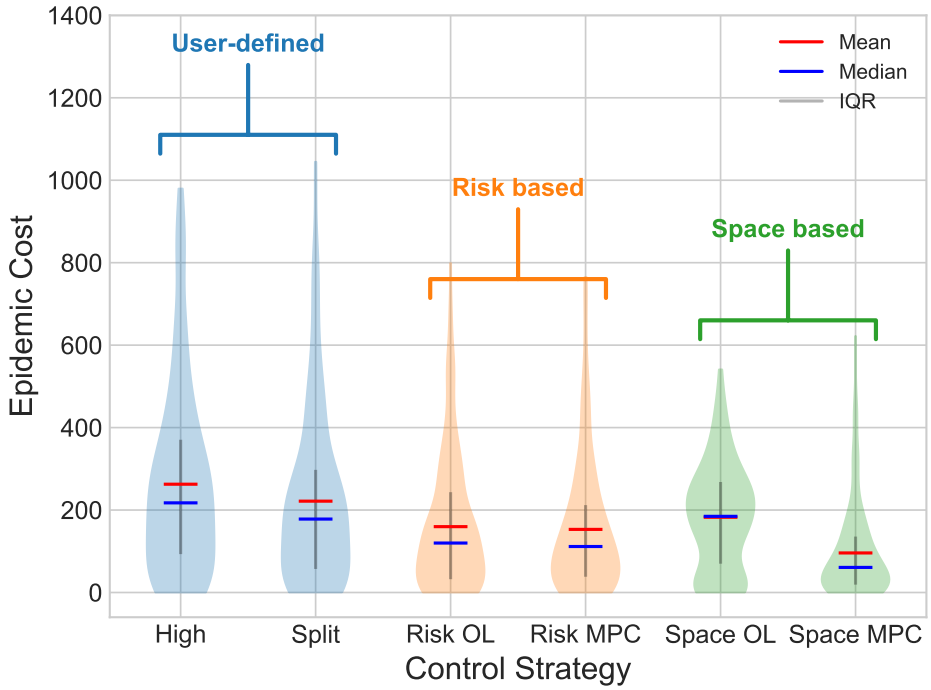


Figure S13: Results of control optimisation scenarios with alternative, more heterogeneous risk structure $\rho_{\text{het}}$.

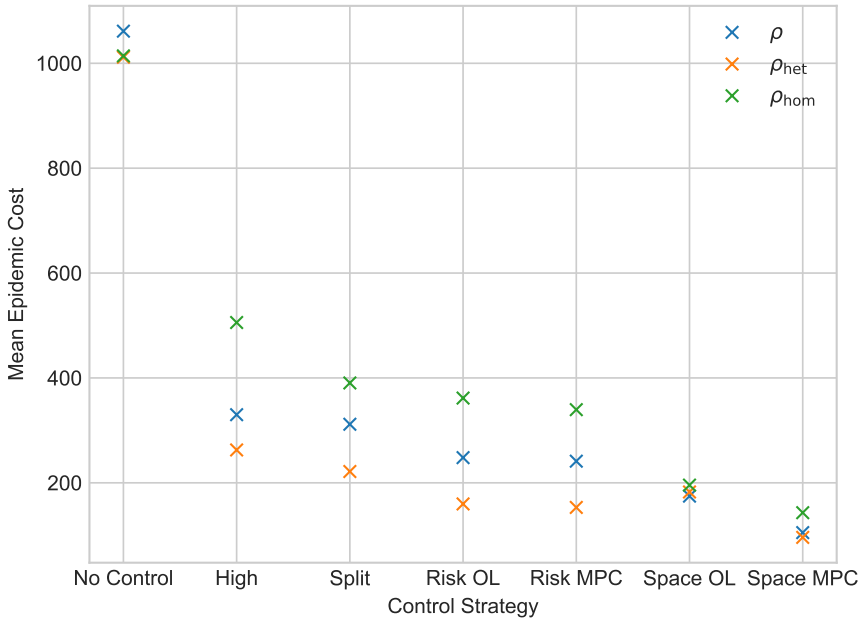


Figure S14: Mean performance of each control strategy using all three risk structures.

# References


[1] Rowthorn RE, Laxminarayan R, Gilligan CA. 2009. Optimal control of epidemics in metapopulations. *J. R. Soc. Interface* **6**, 1135–1144 doi:10.1098/rsif.2008.0402

[2] Keeling MJ, Woolhouse ME, Shaw DJ, Matthews L, Chase-Topping M, Haydon DT, Cornell SJ, Kappey J, Wilesmith J, Grenfell BT. 2001. Dynamics of the 2001 UK foot and mouth epidemic: stochastic dispersal in a heterogeneous landscape. *Science* **294**, 813–817 doi:10.1126/science.1065973

[3] Keeling MJ, Gilligan CA. 2000. Metapopulation dynamics of bubonic plague. *Nature* **407**, 903 doi:10.1038/35038073

[4] Margosian ML, Garrett KA, Hutchinson JS, With KA. 2009. Connectivity of the American agricultural landscape: assessing the national risk of crop pest and disease spread. *BioScience* **59**, 141–151 doi:10.1525/bio.2009.59.2.7

[5] Bansal S, Grenfell BT, Meyers LA. 2007. When individual behaviour matters: homogeneous and network models in epidemiology. *J. R. Soc. Interface* **4**, 879–891 doi:10.1098/rsif.2007.1100

[6] Gillespie DT. 1977. Exact stochastic simulation of coupled chemical reactions. *J. Phys. Chem.* **81**, 2340–2361 doi:10.1021/j100540a008

[7] Bolker BM, 2008. *Ecological models and data in R*. Princeton University Press

[8] Keeling MJ, Rohani P, 2008. *Modeling Infectious Diseases in Humans and Animals*. Princeton University Press

[9] Keeling MJ. 1999. The effects of local spatial structure on epidemiological invasions. *Proc. R. Soc. Lond. B Biol. Sci.* **266**, 859–867 doi:10.1098/rspb.1999.0716

[10] Roy M, Pascual M. 2006. On representing network heterogeneities in the incidence rate of simple epidemic models. *Ecol. Complex.* **3**, 80–90 doi:10.1016/j.ecocom.2005.09.001

[11] Clarke J, White KAJ, Turner K. 2013. Approximating optimal controls for networks when there are combinations of population-level and targeted measures available: chlamydia infection as a case-study. *Bull. Math. Biol.* **75**, 1747–1777 doi:10.1007/s11538-013-9867-9

[12] Stroud PD, Sydoriak SJ, Riese JM, Smith JP, Mniszewski SM, Romero PR. 2006. Semi-empirical power-law scaling of new infection rate to model epidemic dynamics with inhomogeneous mixing. *Math. Biosci.* **203**, 301–318 doi:10.1016/j.mbs.2006.01.007

[13] Bonnans F, Martinon P, Giorgi D, Grélard V, Maindrault S, Tissot O, Liu J, 2017. Bocop 2.0.5 - user guide. http://www.bocop.org/

[14] Betts J, 2010. *Practical Methods for Optimal Control and Estimation Using Nonlinear Programming*. Siam

[15] Lenhart S, Workman JT, 2007. *Optimal Control Applied to Biological Models*. CRC Press

[16] Forster G, Gilligan CA. 2007. Optimizing the control of disease infestations at the landscape scale. *Proc. Natl. Acad. Sci. U.S.A.* **104**, 4984–4989 doi:10.1073/pnas.0607900104